The Meteoritical Society

Meteoritics & Planetary Science 1–14 (2019)
doi: 10.1111/maps.13254

Possible records of space weathering on Vesta: Case study in a brecciated eucrite Northwest Africa 1109

Shu-Zhou WANG[1], Ai-Cheng ZHANG[1,2*], Run-Lian PANG[1], Yang LI[3], and Jia-Ni CHEN[1]

[1]State Key Laboratory for Mineral Deposits Research, School of Earth Sciences and Engineering, Nanjing University, Nanjing 210046, China
[2]Lunar and Planetary Science Institute, Nanjing University, Nanjing 210046, China
[3]Center for Lunar and Planetary Sciences, Institute of Geochemistry, Chinese Academy of Sciences, Guiyang 550081, China
*Corresponding author. E-mail: aczhang@nju.edu.cn

(Received 19 April 2018; revision accepted 07 December 2018)

Abstract–Records of space weathering are important for understanding the formation and evolution of surface regolith on airless celestial bodies. Current understanding of space weathering processes on asteroids including asteroid-4 Vesta, the source of the howardite–eucrite–diogenite (HED) meteorites, lags behind what is known for the Moon. In this study, we studied agglutinates, a vesicular glass-coating lithic clast, and a fine-grained sulfide replacement texture in the polymict breccia Northwest Africa (NWA) 1109 with electron microscopy. In agglutinates, nanophase grains of FeNi and FeS were observed, whereas $npFe^0$ was absent. We suggested that the agglutinates in NWA 1109 formed from fine-grained surface materials of Vesta during meteorite/micrometeorite bombardment. The fine-grained sulfide replacement texture (troilite + hedenbergite + silica) should be a result of reaction between S-rich vapors and pyroxferroite. The unique Fe/Mn values of relict pyroxferroite indicate a different source from normal HED pyroxenes, arguing that the reaction took place on or near the surface of Vesta. The fine-grained sulfide replacement texture could be a product of nontypical space weathering on airless celestial bodies. We should pay attention to this texture in future returned samples by asteroid exploration missions.

INTRODUCTION

The surfaces of airless celestial bodies in the solar system underwent a constant process of space weathering driven predominantly by the effects of solar wind ion irradiation, and meteorite and micrometeorite bombardments (Pieters et al. 2000; Hapke 2001; Clark et al. 2002; Chapman 2004; Pieters and Noble 2016). These processes changed the physical structure, optical properties, and chemical or mineralogical properties of materials on the surface of airless celestial bodies. The term space weathering has been widely used to describe the cumulative effects of these processes that result in the formation and evolution of airless body surface regoliths. Unraveling potential records of space weathering is crucial to constrain the types, diversity, and driving forces of the dynamic processes that were and are prevailing on the surface of airless celestial bodies and important for understanding the evolution history of surface regolith on airless celestial bodies.

One of the significant effects of space weathering is that it strongly affects the remote sensing data of airless celestial bodies and how they are interpreted (Pieters et al. 2000; Hapke 2001; Clark et al. 2002; Chapman 2004; Pieters and Noble 2016). For instance, materials that have been strongly space-weathered usually show reflectance spectra with weak absorption bands and/or reddened reflectance spectra (Pieters and Noble 2016). Therefore, space weathering has become one of the important and active themes in planetary science. The investigations on space weathering mainly include (1) remote sensing and in situ observations of surface materials on airless celestial bodies, (2) observations and analyses of regolith materials with state-of-the-art instruments (e.g., transmission electron microscopes/TEM) in laboratory, and (3) laboratory simulations

with various materials irradiated by lasers and ions (e.g., Noble et al. 2007; Pieters and Noble 2016; Wu et al. 2017).

Current understanding of space weathering records in natural samples largely relies on analyses of lunar regolith returned by the Apollo missions and Itokawa particles returned by the Hayabusa mission (Pieters and Noble 2016). In lunar regolith, the typical space weathering product is nanophase reduced Fe ($npFe^0$). The major scenario for interpreting the formation mechanism of $npFe^0$ particles in lunar regolith: solar wind ion implantation acting in combination with micrometeorite bombardment (Hapke 1973; Hapke et al. 1975; Keller and McKay 1997; Pieters et al. 2000). An additional mechanism involves vaporization and deposition due to micrometeorite impacts (Pieters and Noble 2016). Besides $npFe^0$, recently, Gu et al. (2018) reported the presence of silicon oxide nanoparticles (10–25 nm in grain size) in Apollo 15 lunar soil. Although typical space weathering products are on nanometer scale, the discovery of hapkeite (Fe_2Si) in lunar meteorite Dhofar 280 (Anand et al. 2004) and Apollo 16 sample 61500 (Gopon et al. 2017) indicates that space weathering products are not necessarily nanoscale in grain size. They could be large up to tens of micrometers (Anand et al. 2004).

Space weathering on asteroids is less well understood compared to the Moon. Particles returned from near-Earth asteroid 25143 Itokawa have been intensively studied in recent years (e.g., Noguchi et al. 2011, 2014; Nakamura et al. 2012; Keller and Berger 2014; Thompson et al. 2014; Harries and Langenhorst 2014, 2018; Harries et al. 2016). Noguchi et al. (2011) revealed that the space weathering products on Itokawa contain both $npFe^0$ particles and nanophase sulfide particles. They suggested that both micrometeorite bombardment and solar wind irradiation affected the materials on the surface of Itokawa. However, the space environment in the main asteroid belt between Mars and Jupiter might be different from the inner solar system, including the slower impact speed, the low flux of solar wind, and the greater average impact rate (e.g., Rubin 2015). Therefore, space weathering on asteroids in the main asteroid melt is an important and active subject to be studied.

Asteroid 4-Vesta is the second largest asteroid in the main asteroid belt. It is considered to be the parent body of howardite–eucrite–diogenite (HED) meteorites (McCord et al. 1970; Binzel and Xu 1993; McSween et al. 2011; Russell et al. 2012; McCoy et al. 2015; Mittlefehldt 2015). Different from the Moon and other asteroids, the spectra of materials on the Vestan surface are comparable to HED meteorites with relatively little optical changes due to space weathering (e.g., Hiroi et al. 1994; Russell et al. 2012). This is surprising because Vesta is one of the oldest protoplanets in the solar system and its surface potentially exposed to the space environment for billion years. To interpret the absence of space weathering on Vesta, two scenarios have been proposed in previous investigations (Fu et al. 2012; Pieters et al. 2012). Pieters et al. (2012) suggested that Vesta's surface does not exhibit lunar-like space weathering (involving abundant nanophase iron) due to its location and bulk mineralogy, but that Vestan surface weathering as observed by Dawn is instead dominated by minor contamination and regolith mixing. However, Fu et al. (2012) suggested that an earlier dynamo had protected Vesta from space weathering, based on the remnant magnetization in Allan Hills A81001. In howardite meteorite Kapoeta, Noble et al. (2010) identified glass rims, agglutinates (fragments where small particles are bonded by vesicular glass; McKay et al. 1991; Papike et al. 1998), and possible nanophase particles in the rim of pyroxene grains. Liu et al. (2015) described a few agglutinates and vesicular coatings in the NWA 1769 howardite, where $npFe^0$, and nanophase grains of FeNi and FeS were identified.

To further understand the presence and diversity of space weathering products on Vesta, we studied a polymict breccia Northwest Africa (NWA) 1109. In NWA 1109, we observed the presence of a few agglutinates and lithic clasts that contain fine-grained mineral assemblage of troilite, hedenbergite, and silica. In this study, we describe their petrography and mineralogy and discuss the possibility that they are space weathering products formed on Vesta.

SAMPLES AND ANALYTICAL METHODS

Two polished sections of NWA 1109 were used in this study. Their petrographic textures were observed with scanning electron microscopes (SEM; JEOL JSM-6490 and Zeiss Supra 55) using backscattered electron (BSE) imaging mode at Nanjing University, China. Both of the SEM instruments were operated at an accelerating voltage of 15 kV. Identification of minerals and elemental X-ray mapping were performed using energy-dispersive spectrometer (EDS) detectors installed on these two SEM instruments.

The chemical composition of minerals was measured using a JEOL 8100 electron probe microanalyzer (EPMA) equipped with four wavelength dispersive spectrometers (WDS) at Nanjing University. The measurements were mainly made at an accelerating voltage of 15 kV and a beam current of 20 nA. A defocused beam (~5 μm) was used for plagioclase and silicate glass. For other phases, a focused beam was used. In order to measure fine-grained minerals (<2 μm in size),

an accelerating voltage of 10 kV and a beam current of 20 nA was used. Peak and background measurement times are 20 s and 10 s, respectively. Concentrations of Si, Ti, Al, Cr, Fe, Mn, Mg, Ca, Na, and K were calibrated with both natural and synthetic standards. All results were reduced with the ZAF procedure for the JEOL microprobe instrument.

To confirm the crystal structure of pyroxferroite in this study, we have performed electron backscatter diffraction (EBSD) with the detector installed on the FEG-SEM instrument at Hokkaido University, Japan. The EBSD patterns were collected and indexed with the Aztec software. The potential pyroxferroite was indexed with the structures of enstatite, pigeonite, hedenbergite, and rhodonite, but only can be indexed by the triclinic rhodonite structure with a mean angle deviation (MAD) value down to 0.41.

An ultra-thin foil was excavated with a focused ion beam (FIB) system from an agglutinate in NWA 1109. The FIB preparation was conducted on FEI Scios Dual Beam at the Institute of Geochemistry, Chinese Academy of Sciences, Guiyang, China. First, a 2 μm layer of Pt was deposited on the sample to protect the surface. Then, initial sectioning was made under 30 kV and 15 nA. After the foil was lifted out from the polished section and attached to a copper grid using Pt deposition, it was milled with a beam current in the order of 1 nA, 500 pA, and 300 pA, respectively. The final foil was approximately 100 nm in thickness. The texture and mineralogy were studied using a FEI Tecnai F20 transmission electron microscope (TEM) at Nanjing University. The TEM measurement was conducted under 200 kV. Bright field TEM observation, energy-dispersive X-ray analyses, X-ray elemental mapping, and high-angle annular dark field-scanning transmission electron microscope (HAADF-STEM) observations were performed.

RESULTS

Petrography and Mineralogy of NWA 1109

Petrography and mineralogy of NWA 1109 have been described in our previous investigation (Pang et al. 2017), but are briefly redescribed here. The NWA 1109 meteorite is mainly composed of mineral fragments and a few lithic clasts (Fig. 1), which have a large variation in size from a few micrometers to approximately 1 mm. The lithic clasts contain basaltic, diogenitic, and impact-melt lithic clasts. The mineral fragments are dominated by pyroxene and plagioclase. Fayalitic olivine, silica, ilmenite, chromite, FeNi metal, phosphate, and troilite mainly occur as accessory minerals. Generally, eucritic components are dominant in NWA 1109 (Fig. 1).

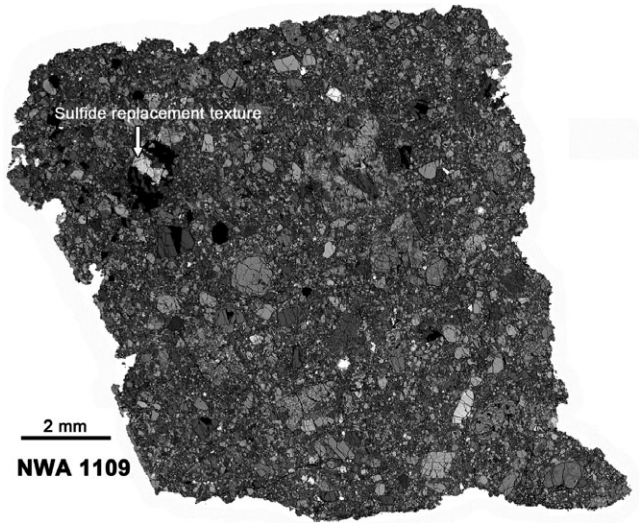

Fig. 1. Mosaic backscattered electron image of a thin section of NWA 1109.

Lithic Clasts with a Vesicular Texture

Four lithic clasts with a vesicular texture have been observed in this study. In three of them, irregular mineral fragments are bonded by vesicular glass (Fig. 2). According to the definition of agglutinate by McKay et al. (1991) and Papike et al. (1998), they are agglutinate clasts. The another lithic clast has a vesicular coating (Fig. 3). All of the three agglutinate clasts are individual clasts and show different shapes. Their sizes vary from ~70 to ~300 μm (Fig. 2). They consist of vesicular glass enclosing grain fragments of pyroxene/pyroxenoid, plagioclase, olivine, and a silica phase. The pyroxene/pyroxenoid fragments within vesicular glass have a large variation in textures and chemical compositions ($En_{17.4\text{-}73.4}Fs_{24.0\text{-}59.6}Wo_{2.6\text{-}25.9}$). In the agglutinate shown in Fig. 2a, pyroxene grains with and without exsolution lamellae are observed. However, in the agglutinate shown in Fig. 2c, pyroxene has a large chemical variation (orthopyroxene to subcalcic augite) among different grains although no exsolution lamellae are observed. Fine FeNi metal grains (<1 μm) are also present. A schlieren texture is also present in one of the agglutinates (Fig. 2b). Vesicles in these agglutinates vary in size from ~2 μm to ~10 μm. Figure 4a shows a HAADF-STEM image of a TEM foil cut from the agglutinate shown in Fig. 2d. The TEM-EDS mapping results reveal the presence of both nanophase FeNi (<2 wt% Ni) and Fe-sulfide grains in glass (Fig. 4). Their grain sizes vary from a few nanometers to approximately 50 nm. However, no $npFe^0$ was observed.

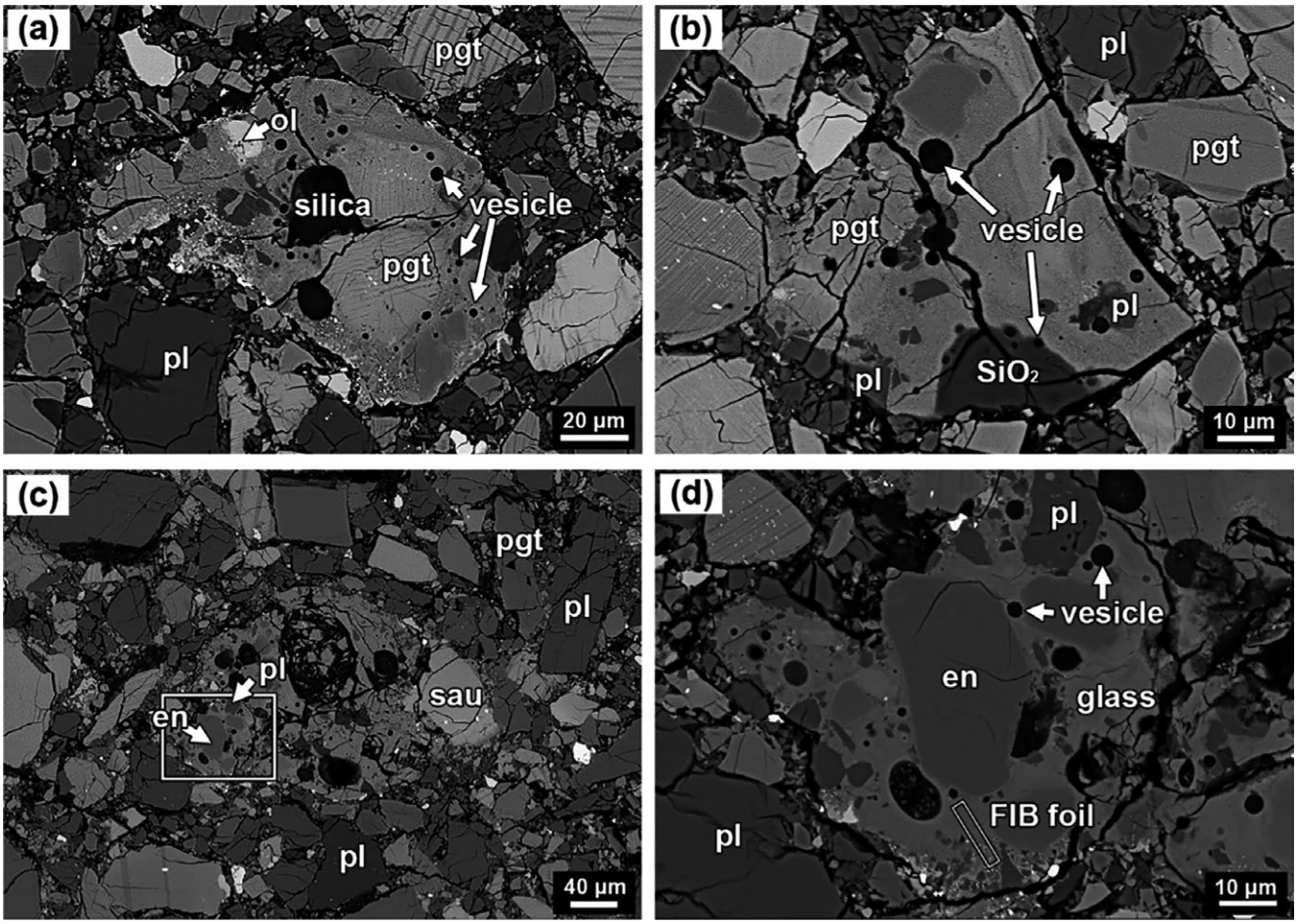

Fig. 2. BSE images of agglutinates in NWA 1109. a) Both pyroxene grains with and without exsolution lamellae are enclosed within vesicular glass. b) The vesicular glass shows a schlieren texture. c) A large agglutinate that contains pyroxene grains with a large difference of mineral composition. d) Magnified image of the rectangle outline in (c). The rectangle in (d) indicates the position where the FIB foil was cut. Ol = olivine; pgt = pigeonite; en = enstatite; sau = subcalcic augite; pl = plagioclase.

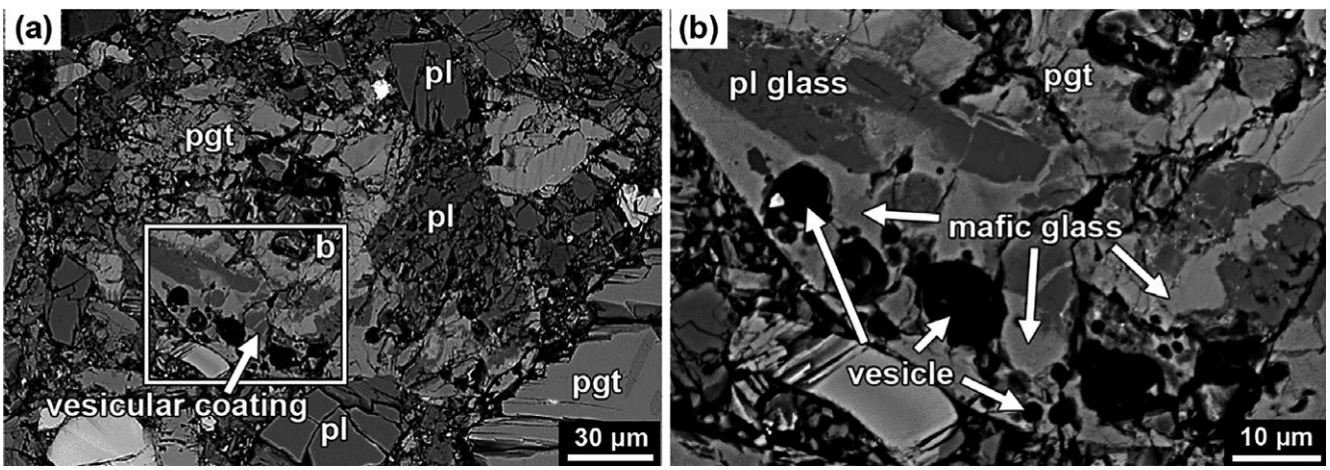

Fig. 3. a) BSE image of the lithic clast with vesicular coating in NWA 1109. b) Magnified image of the rectangle outline in (a). Pgt: pigeonite, pl: plagioclase.

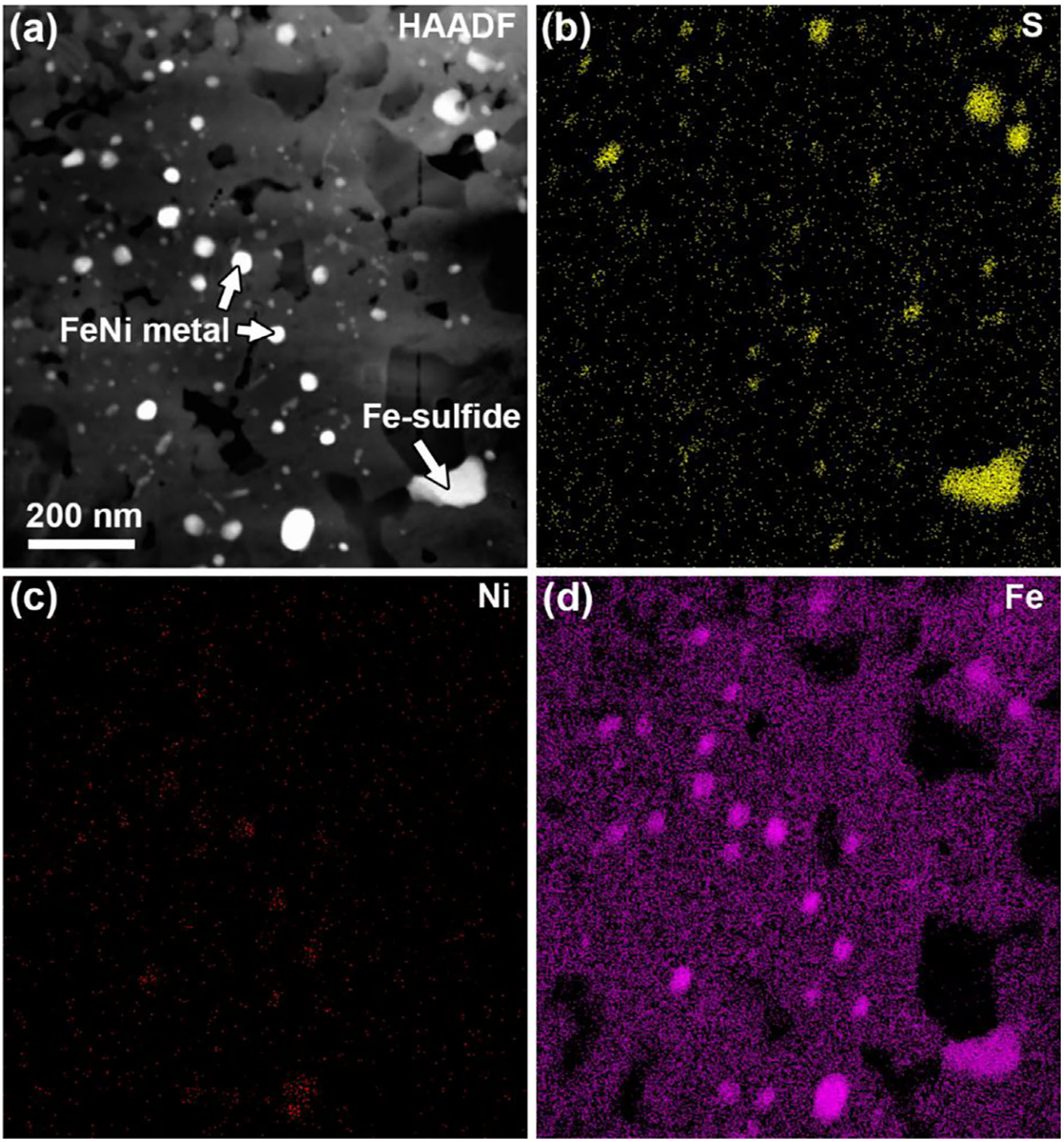

Fig. 4. HAADF image (a) and X-ray elemental mapping results (b–d) of the FIB foil cut in the agglutinate shown in Fig. 2d.

The lithic clast with vesicular coating is present in the interior of a petrologic thin section of NWA 1109 and surrounded by fragments of plagioclase and pyroxene (Fig. 3). It is irregular in shape and about 170 μm across. This clast consists mainly of Fe-rich pigeonite and plagioclase fragments with fractures. The pigeonite and plagioclase fragments are partially covered by a mafic glassy crust (Fig. 3). The glassy crust is approximately 50 μm in thickness and has a smooth surface. Abundant spherical vesicles (from submicron to 12 μm in diameter) are present along the outer rim of the glassy crust. A few irregular

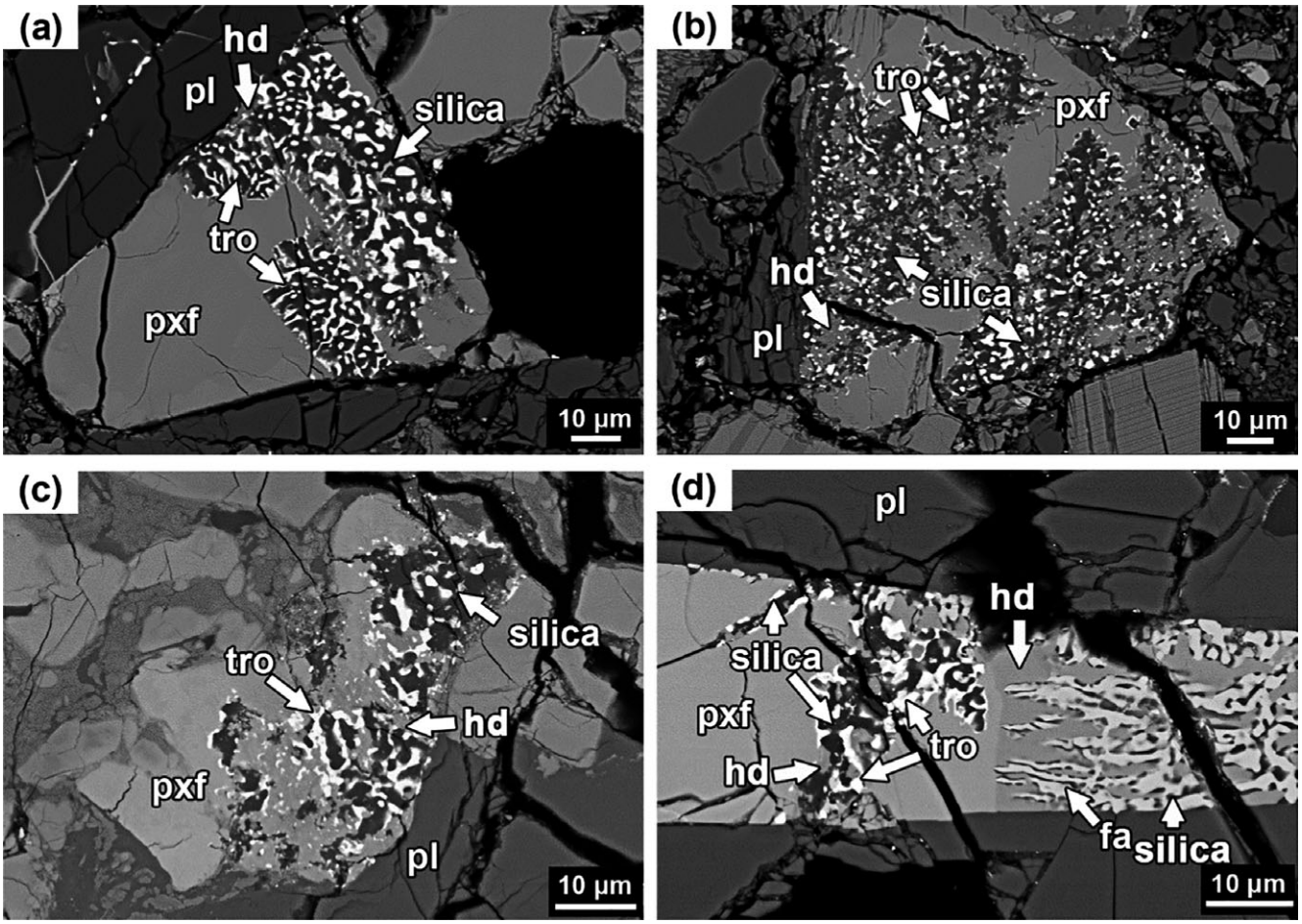

Fig. 5. BSE images of mineral and lithic fragments with sulfide replacement texture. Note that the left and right portions in (d) have different textures and mineral assemblages. Fa = fayalite; pxf = pyroxferroite; hd = hedenbergite; pl = plagioclase; tro = troilite.

plagioclase-glass fragments (8–30 μm in size) are present in the glass crust along its inner rim. These plagioclase-glass fragments contain MgO + FeO up to 5.1 wt%, differing from plagioclase (MgO + FeO <0.9 wt%) that is closely associated with pigeonite. The average composition of the mafic glass mainly contains 20.7 wt% FeO, 11.2 wt% MgO, 10.8 wt% Al_2O_3, and 8.0 wt% CaO. A few fractures within the plagioclase fragments are filled with mafic glass (Fig. 3b).

Fine-Grained Sulfide Replacement Textures

Several lithic and mineral fragments with a sulfide replacement texture were found in NWA 1109 (Figs. 5 and 6). Fine-grained troilite, hedenbergite, and silica form a vermicular texture replacing a coarse-grained pyroxferroite (Figs. 5 and 6). The structural identification and mineral compositions of pyroxferroite are shown in Fig. 7 and Table 1. The fine-grained minerals in the sulfide replacement texture have similar grain sizes (1–5 μm). The fine-grained mineral assemblages have irregular boundaries with the relict pyroxferroite. Minor, fine-grained, and irregular Fe-rich olivine (~3 μm) is present in one of the lithic clasts with the sulfide replacement texture (Figs. 6d and 6f). In one of the lithic clasts with the sulfide replacement texture, a vermicular symplectite of fayalite, hedenbergite, and silica was also observed (Fig. 5d). Note that the symplectite of fayalite, hedenbergite, and silica has a sharp boundary with the pyroxferroite grain that has been partially replaced by hedenbergite, troilite, and silica.

Most of the relict pyroxferroite grains have similar chemical compositions ($En_{3.1–8.7}Fs_{75.9–82.2}Wo_{13.7–16.4}$); however, in one of the lithic clasts, the coarse-grained pyroxferroite has higher Wo components ($En_{3.8–5.4}Fs_{66.8–74.9}Wo_{19.7–29.4}$; Fig. 8; Table 1). Elemental X-ray mapping shows a decreasing trend of Mg concentration from the boundary between pyroxferroite and the fine-grained mineral assemblage to the inner

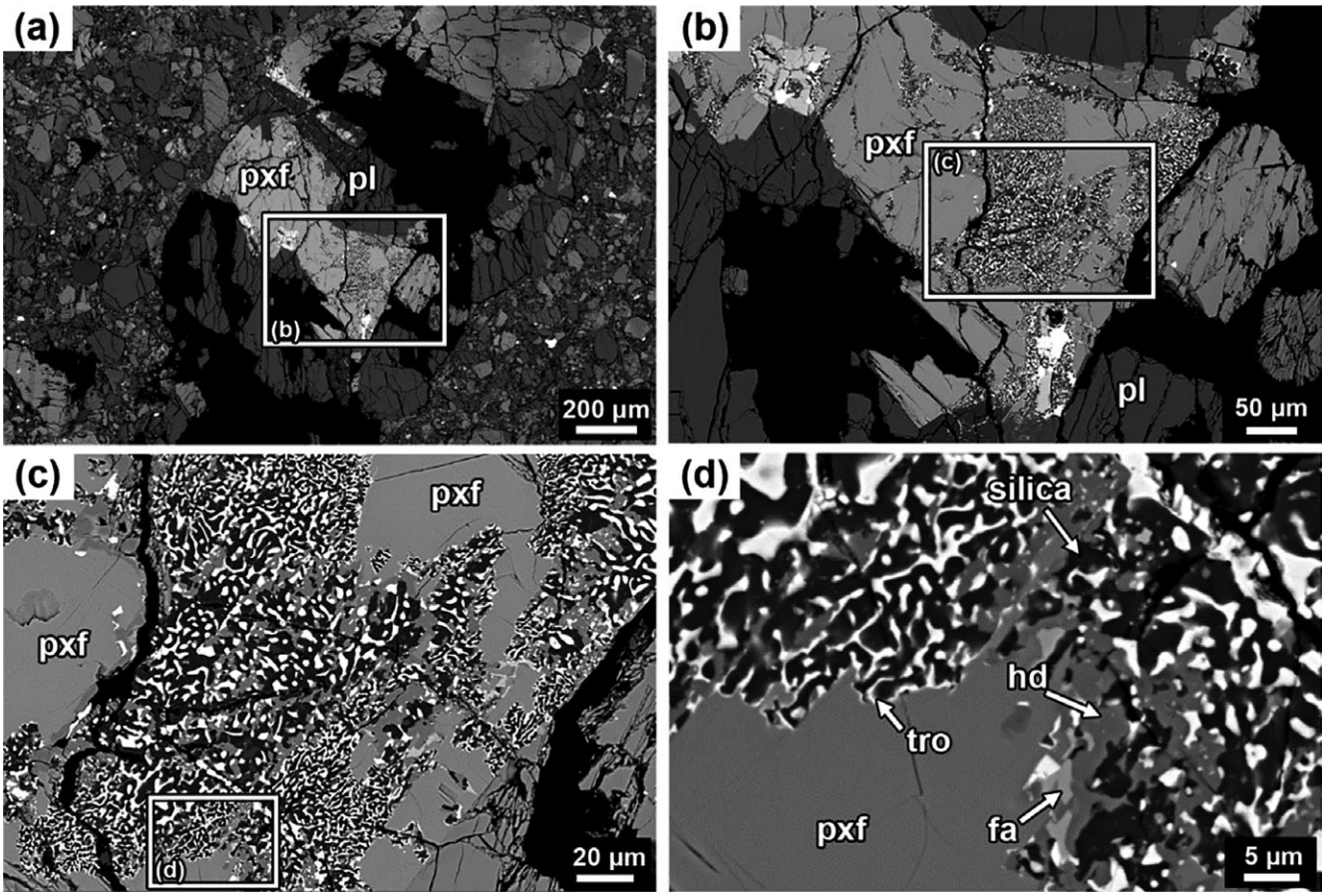

Fig. 6. BSE images of a large lithic clast with sulfide replacement texture. a) The outline of the lithic clast. b) Magnified image of the pyroxene grain with sulfide replacement texture shown in (a). c) Magnified image of the rectangular outline in (b). It shows that pyroxferroite grains have been heterogeneously replaced by fine-grained mineral assemblage. d) Magnified image of the rectangular outline in (c). It shows an irregular boundary between relict pyroxferroite and fine-grained mineral assemblage of troilite, hedenbergite, silica, and minor fayalite. fa = fayalite; pxf = pyroxferroite; hd = hedenbergite; pl = plagioclase; tro = troilite.

part of pyroxferroite (Fig. 9f). Most of the pyroxferroite grains have a large variation in Fe/Mn value (14–30) among different lithic clasts and the compositions plot above the trend line for pyroxene in HED meteorites (Fig. 10). However, the pyroxferroite with higher Wo components has higher Fe/Mn values (32–48), even higher than the typical value (~30) for HED pyroxenes (Papike et al. 2003). The chemical compositions of hedenbergite in the fine-grained mineral assemblage are $En_{4.3–7.3}Fs_{44.7–53.4}Wo_{43.0–48.0}$ (Fig. 8). The Fe/Mn values of hedenbergite (26–57) are close to and slightly higher than the typical value for HED pyroxenes. It is noteworthy that Mn is depleted in the region with sulfide replacement texture compared to the relict pyroxferroite grains (Fig. 9h). Fine-grained olivine that is closely associated with the sulfide replacement texture is dominated by fayalite component ($Fa_{94–98}$).

DISCUSSION

Origin of Lithic Clasts with Vesicular Textures

Agglutinates are common components in lunar regolith. The presence of nanophase Fe grains in both the metallic and recently discovered nonmetallic state is the key feature in lunar agglutinates that distinguishes them from simple impact glass (McKay et al. 1991; Thompson et al. 2016). In this study, the agglutinates contain pyroxene grains with large variations in texture and mineral compositions and other minerals such as plagioclase, olivine, and a silica phase. This feature suggests that these agglutinate clasts are melted products of regolith materials, probably due to meteorite/micrometeorite bombardments. This feature also differentiates them from fragments of heavily shocked rocks, where pyroxene grains should a common source.

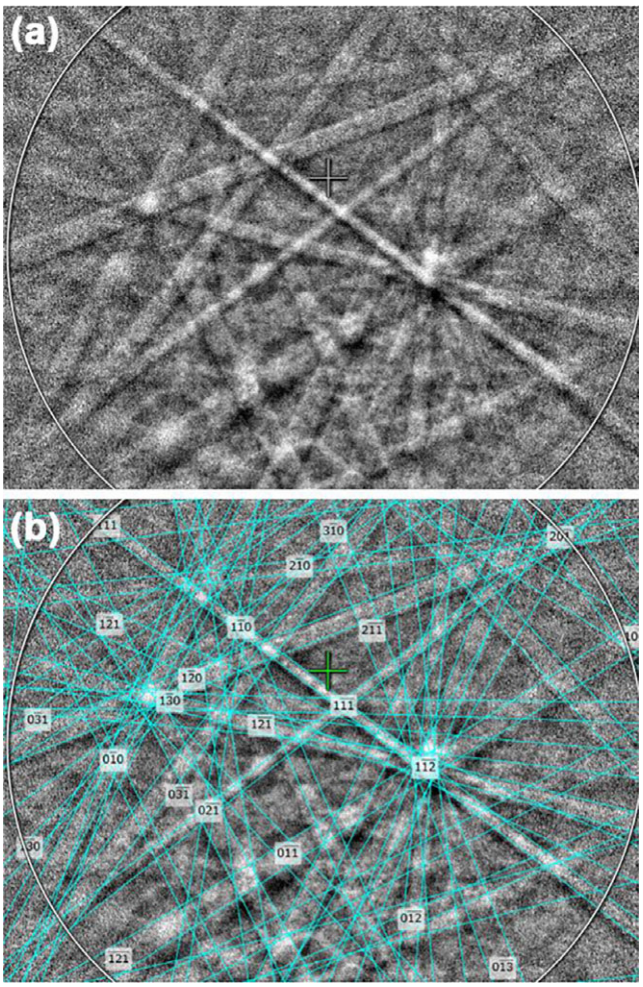

Fig. 7. Electron backscatter diffraction pattern of pyroxferroite in NWA 1109 and the pattern indexed with the triclinic rhodonite structure (MAD = 0.41).

Clasts interpreted as regolith agglutinates have been reported in howardite meteorites Kapoeta and NWA 1769 (Noble et al. 2010; Liu et al. 2015). Those described by Noble et al. (2010) in Kapoeta are comparatively small in size (5–15 μm). However, the agglutinates described by Liu et al. (2015) are much larger in size (300–450 μm). The agglutinates in this study texturally resemble those reported in Liu et al. (2015). The difference is that opaque minerals in NWA 1769 are nanophase Fe^0, FeS, and FeNi grains (Liu et al. 2015). However, opaque minerals in the agglutinates in NWA 1109 contain only nanophase grains of FeS and FeNi. No $npFe^0$ grains were observed in this study. It should be noted that FeNi grains in the agglutinates in NWA 1109 contain low concentrations of Ni (<2 wt%). This Ni concentration is between $npFe^0$ and meteoritic FeNi metal (>2 wt%; Brearley and Jones 1998). The absence of $npFe^0$ and the low Ni concentrations of FeNi metal could be a mixing product of space-weathered $npFe^0$ and chondritic FeNi metal grains. FeNi metal grains have been observed in space-weathered lunar meteorite (Anand et al. 2004) and laser-bombarded products of ordinary chondrites (Wu et al. 2017).

Although only a few agglutinates have so far been found in HED meteorites (Noble et al. 2010; Liu et al. 2015; this study), they show an important difference from lunar agglutinates. Nanophase Fe^0 grains are the main opaque minerals in space weathering products in lunar agglutinates. However, nanoscale grains of FeS and FeNi are more commonly observed in the agglutinate from HED meteorites. Besides potential difference of mechanisms of forming $npFe^0$ in agglutinates (solar wind irradiation versus meteorite/micrometeorite bombardment; Hapke 1973; Hapke et al. 1975; Keller and McKay 1997; Pieters et al. 2000), we suspect that different average impact velocities of meteorites/micrometeorites on the Moon and Vesta could be one reason. The average impact velocity of meteorites/micrometeorites on the Moon is much higher than that of on asteroids in the Main Belt (Davis et al. 1989). High impact velocity of meteorites/micrometeorites on the Moon led to the vaporization or loss of sulfur to space, whereas such effect could be much weaker on Vesta, which had comparatively low impact velocity. This speculation seems supported by the fact that many brecciated feldspathic lunar samples contain 0.5 to 2 wt% chondritic components (Korotev et al. 2003); however, chondritic components are very seldom observed in brecciated feldspathic lunar samples (Joy et al. 2012). Instead, chondritic components have a higher frequency of occurrence in HED meteorites (Zolensky et al. 1996).

Formation Mechanism of Sulfide Replacement Textures

Mesostasis materials in some basaltic eucrites and hedenbergite–fayalite–silica symplectites are more or less similar to the sulfide replacement texture in mineralogy, grain size, and texture. However, they are of different origins (Zhang et al. 2013). (1) Mesostasis in basaltic eucrites is the late-stage interstitial materials among early crystallized phases (such as pyroxene and plagioclase) and usually has a sharp boundary with surrounding minerals. This is contrasted with the sulfide replacement texture which is present in pyroxene (Zhang et al. 2013) or pyroxenoid (this study). (2) Hedenbergite–fayalite–silica symplectite is common in lunar and HED meteorites (Joy et al. 2008; Liu et al. 2009). However, the constituent minerals in the hedenbergite–fayalite–silica symplectite usually have comparable modal abundances, which are largely distinct from the sulfide replacement texture. In the

Table 1. Representative EPMA results (wt%) of pyroxferroite, hedenbergite, and fayalite in sulfide replacement textures.

	Pyroxferroite					Hedenbergite					Fayalite
SiO_2	46.3	46.0	46.3	46.1	46.6	47.6	48.4	48.4	48.2	48.5	30.4
TiO_2	0.42	0.47	0.46	0.49	0.49	0.16	0.34	0.22	0.29	0.17	0.23
Al_2O_3	0.40	0.34	0.41	0.32	0.27	0.52	0.32	0.69	0.64	0.47	0.04
Cr_2O_3	0.02	bd	0.02	bd	0.02	0.03	0.09	0.06	0.18	0.12	bd
MgO	1.48	1.17	1.39	1.40	2.44	1.42	1.68	2.00	1.56	1.84	1.54
FeO	42.3	43.0	42.7	42.2	40.9	28.2	29.6	26.3	28.6	28.4	64.6
MnO	2.33	2.10	2.69	2.72	2.64	0.64	0.88	0.80	0.64	0.54	1.59
CaO	6.61	6.40	6.31	6.59	6.68	20.7	19.2	20.8	20.6	20.3	1.06
Na_2O	0.02	bd	0.04	bd	bd	bd	0.04	0.03	bd	0.02	0.04
K_2O	bd	bd	bd	bd	bd	0.05	bd	0.05	bd	bd	0.03
Total	99.88	99.48	100.32	99.82	100.04	99.32	100.55	99.35	100.71	100.36	99.53
Si	1.977	1.977	1.973	1.974	1.975	1.974	1.982	1.985	1.968	1.981	1.014
Ti	0.013	0.015	0.015	0.016	0.016	0.005	0.010	0.007	0.009	0.005	0.006
Al	0.020	0.017	0.021	0.016	0.014	0.025	0.015	0.033	0.030	0.022	0.002
Cr	0.001	bd	0.001	bd	0.001	0.001	0.003	0.002	0.006	0.004	bd
Mg	0.095	0.075	0.089	0.090	0.155	0.088	0.103	0.123	0.096	0.113	0.077
Fe	1.505	1.543	1.517	1.505	1.444	0.973	1.012	0.898	0.972	0.968	1.796
Mn	0.084	0.076	0.097	0.098	0.095	0.022	0.030	0.028	0.022	0.019	0.045
Ca	0.303	0.295	0.288	0.302	0.303	0.918	0.841	0.913	0.902	0.887	0.038
Na	0.002	bd	0.003	bd	bd	bd	0.003	0.002	bd	0.002	0.003
K	bd	bd	bd	bd	bd	0.002	bd	0.002	bd	bd	0.001
sum	4.000	3.998	4.004	4.001	4.003	4.008	3.999	3.993	4.005	4.001	2.982
Fe/Mn	17.9	20.3	15.6	15.4	15.2	44.2	33.7	32.1	44.2	50.9	Fa 96
Mg#	5.9	4.6	5.5	5.6	9.7	8.3	9.2	12.0	9.0	10.5	

Mg# = 100 × Mg/(Mg + Fe) in mole. Cations in pyroxferroite and hedenbergite are calculated based on six O atoms, and cations in fayalite are calculated based on eight O atoms.
Bd = below detection limit.

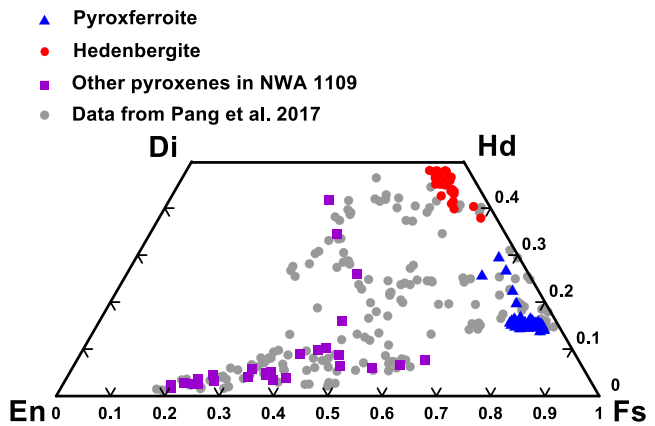

Fig. 8. The compositions of pyroxenes and pyroxenoid in NWA 1109. Blue triangles indicate relict pyroxferroite; red circles indicate fine-grained hedenbergite in sulfide replacement texture; purple squares indicate other pyroxenes in NWA 1109 measured in this study; gray circles are data from Pang et al. (2017).

sulfide replacement texture, fayalite is very rare. Figure 5d in this study shows a coexistence of both the hedenbergite–fayalite–silica symplectite and the sulfide replacement texture; however, they show distinct mineral assemblages and textures.

Sulfide replacement textures that are similar to those in NWA 1109 have been reported in different types of meteorites in the literature (Tomeoka et al. 1992; Patzer and McSween 2012; Shearer et al. 2012; Zhang and Yurimoto 2013; Zhang et al. 2013, 2018; Goodrich et al. 2017). Although there are some differences between modal mineralogy and mineral compositions among these textures, the occurrences of replacement texture and the manner of the occurrence of the sulfides are similar. Several scenarios have been proposed to interpret the formation of the texture; i.e., (1) reaction between sulfide-rich vapors and rocks (Shearer et al. 2012; Zhang and Yurimoto 2013; Zhang et al. 2013, 2018; Goodrich et al. 2017); (2) shock-induced partial melting and quenching (Patzer and McSween 2012); (3) heating events and subsequent recrystallization (Tomeoka et al. 1992).

Shearer et al. (2012) have reported sulfide replacement textures in Apollo lunar samples. Olivine grains in these textures were replaced by sulfide and low-Ca pyroxene. They suggested that these sulfide replacement textures were formed by reaction between

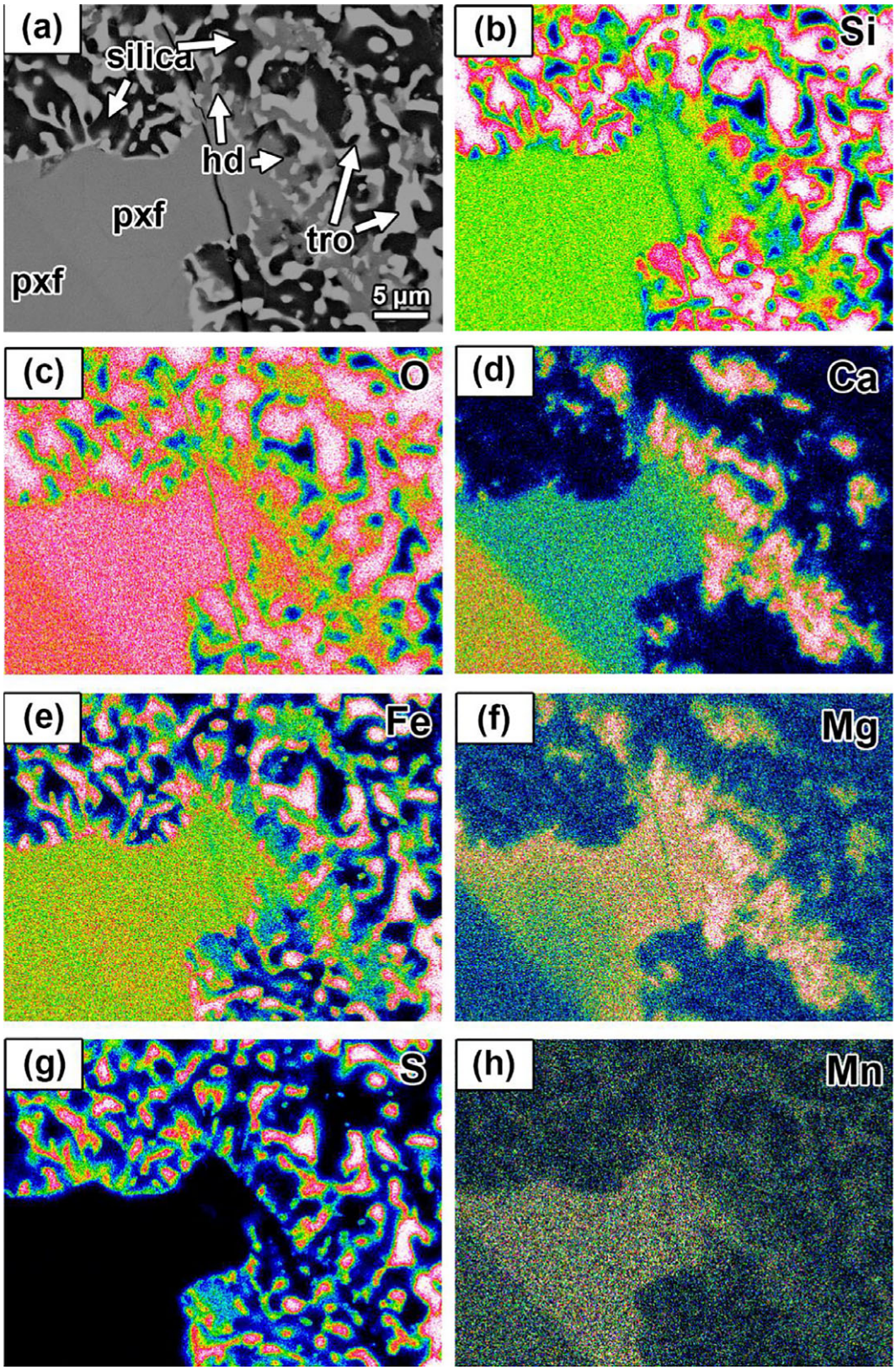

Fig. 9. BSE image (a) and X-ray elemental mapping results (b–h) of a typical region with sulfide replacement texture. Fa = fayalite; pxf = pyroxferroite; pgt = pigeonite, hd = hedenbergite, tro = troilite. For the X-ray mapping results, the color change from dark blue to red and white indicates an increase of counts of each element.

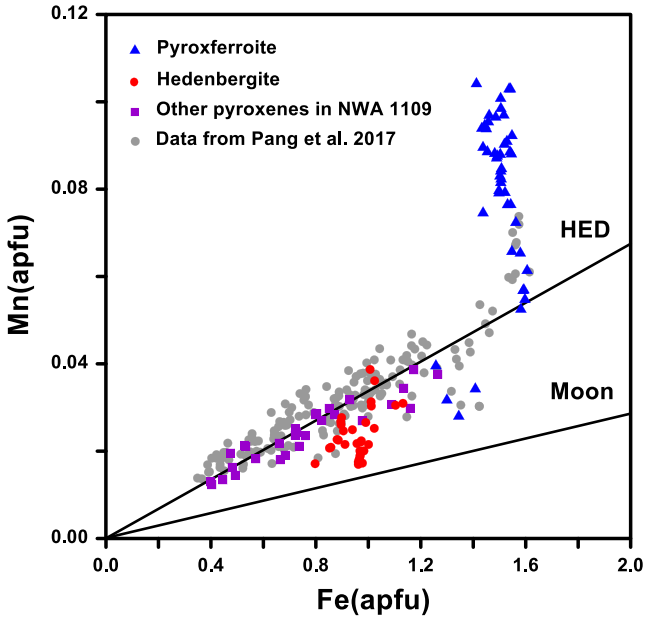

Fig. 10. Fe-Mn compositions of pyroxene in NWA 1109. Blue triangles indicate relict pyroxferroite; red circles indicate fine-grained hedenbergite in sulfide replacement texture; purple squares indicate other pyroxenes in NWA 1109 measured in this study; gray circles are data from Pang et al. (2017). The trend lines for HED meteorites and the Moon are adopted from Papike et al. (2003).

S-rich vapors and rocks in shallow crust of the Moon. The vapor probably formed by degassing of magmas emplaced into the shallow crust and was enriched in S. The vapor–rock reaction mechanism seems to be the most likely explanation for such textures in NWA 1109. However, Vesta was so small compared with the Moon and their magmatic histories are quite different. No volcanic glass has been reported to prove that there are similar magmatic processes on Vesta. Zhang et al. (2013) reported almost identical textures in eucrite NWA 2339. According to distinct Fe/Mn values between relict Fe-rich pigeonite and HED pyroxenes, they suggested that the sulfide replacement texture was not a product of indigenous process on Vesta. Shown in Fig. 10, the Fe/Mn values of relict pyroxferroite in sulfide replacement texture in NWA 1009 are distinctly different from the typical Fe/Mn values for HED pyroxenes (Papike et al. 2003; McSween et al. 2011). This feature is similar to that of pyroxene in NWA 2339 studied by Zhang et al. (2013), although the relict pyroxene has chemical composition (pyroxferroite) different from that (Fe-rich pigeonite and subcalcic augite) reported in Zhang et al. (2013). The distinctly different Fe/Mn values suggest that the pyroxferroite in NWA 1109 could have a source different from normal HED pyroxenes. This would exclude the possibility that the fine-grained mineral assemblage containing troilite had formed in the interior of Vesta. Instead, it is more likely that the reaction between S-rich vapors and pyroxferroite took place on the surface or near the surface of Vesta (Zhang et al. 2013).

Possibility of Nontypical Space Weathering

Space weathering is thought to be common on the surface of airless celestial bodies. However, unlike returned samples of lunar soils and Itokawa grains where the surfaces exposed to the space environment can be directly examined, the only samples we have from other solar system asteroids are the valuable meteorites. However, many meteorites have experienced various degrees of aqueous alteration, thermal metamorphism, and shock metamorphism. It is difficult to firmly determine which textures and products could be related to space weathering and whether they are rare, or common, or extensive across the parent body. Currently, the best way to infer which textures and products are related to space weathering might be a comparison of textures that are present in various meteorites and could also be related to surface process.

The products of space weathering on the Moon provide a reference against which space weathering on other solar system airless bodies can be compared. The key products include the formation of npFe^0 in both agglutinate glass and grain rims, and the agglutinates themselves. Except in agglutinates, npFe^0, Si-oxide grains, and amorphous rims of some minerals (e.g., plagioclase, ilmenite) are usually nanometer-sized in scale (Pieters and Noble [2016] and references therein; Gu et al. 2018). However, Anand et al. (2004) reported a new mineral called "hapkeite," Fe_2Si, in a feldspathic lunar meteorite Dhofar 280. The hapkeite grain is approximately 35 μm. They demonstrated that this mineral could be the product of vapor deposition in lunar soil, a space weathering product. If their interpretation is correct, it is not necessary that space weathering products should be nanoscale in size, although nanophase particles are common in space weathering products. Taylor et al. (2004) reported a texture that fayalite grains were reduced to Fe-metal and silica. They suggested that the texture formed due to reaction between solar wind hydrogen and fayalite on the lunar surface. Although they did not explicitly state that the texture is a record of space weathering, the reaction between solar wind hydrogen and fayalite implies that it is a kind of space weathering. The grain sizes of space weathering products could be a function of nucleation and growth kinetics of various minerals.

With the above discussion in mind, the sulfide replacement texture in NWA 1109 might also be a type of space weathering product. The fine-grained troilite is

comparable in grain size to Fe-metal described in Taylor et al. (2004). The geological setting in which the reaction between S-rich vapor and pyroxene or pyroxenoid took place on or near the surface of Vesta also supports this possibility. Similar sulfide replacement textures in meteorites were not very rare and had been reported in the literature (Patzer and McSween 2012; Shearer et al. 2012; Zhang and Yurimoto 2013; Zhang et al. 2013, 2018; Goodrich et al. 2017). The fine-grained sulfide replacement texture has been observed not only in HED meteorites but also in returned lunar samples (Shearer et al. 2012), brachinite-like achondrites (Goodrich et al. 2017), and carbonaceous chondrites (Tomeoka et al. 1992; Zhang and Yurimoto 2013). These observations suggest that the sulfide replacement textures are widespread among different airless bodies. Although the mineral assemblages of the sulfide replacement textures are different in different meteorites, they probably share a similar formation mechanism that S-rich vapor reacts with certain precursor minerals. Therefore, sulfide replacement might be a common process that was prevailing on the surface of different asteroids. If the sulfide replacement texture is a nontypical product of space weathering, it might be observed in future returned samples by asteroid exploration missions (e.g., OSIRIX-REX and Hayabusa 2).

SUMMARY

In this study, we reported the occurrence of agglutinates, vesicular glass-coating lithic clast, and fine-grained sulfide replacement texture in a brecciated eucrite NWA 1109. The agglutinates contain nanophase grains of FeNi and FeS as major opaque minerals, different from those in lunar regolith. The sulfide replacement texture indicates a reaction between S-rich vapors and pyroxferroite. We argued that the agglutinates and the fine-grained sulfide replacement texture are probably records of space weathering on Vesta. The latter could be a nontypical product of space weathering among airless celestial bodies.

Acknowledgments—This study was financially supported by Natural Science Foundation of Jiangsu Province of China (BK20170017) and National Natural Science Foundation of China (41673068). We thank Prof. Hisayoshi Yurimoto and Dr. Naoya Sakamoto at Hokkaido University for allowing ACZ accessing the FE-SEM in their group. Comments from Dr. Roy Christoffersen and AE Prof. Carle Pieters greatly improved the manuscript.

Editorial Handling—Dr. Carle Pieters

REFERENCES

Anand M., Taylor L. A., Nazarov M. A., Shu J., Mao H. K., and Hemley R. J. 2004. Space weathering on airless planetary bodies: Clues from the lunar mineral hapkeite. *Proceedings of the National Academy of Sciences* 101:6847–6851.

Binzel R. P. and Xu S. 1993. Chips off of asteroid 4 Vesta: Evidence for the parent body of basaltic achondrite meteorites. *Science* 260:186–191.

Brearley A. J. and Jones R. H. 1998. Chondritic meteorites. In *Planetary materials*, edited by Papike J. J. Reviews in Mineralogy, vol. 36. Washington, D.C.: Mineralogical Society of America. pp. 3-1–3-398.

Chapman C. R. 2004. Space weathering of asteroid surfaces. *Annual Reviews of Earth Planetary Science* 32:539–567.

Clark B. E., Hapke B., Pieters C., and Britt D. 2002. Asteroid space weathering and regolith evolution. In *Asteroids III*, edited by Bottke W. F., Cellino A., Paolicchi P., and Binzel R. P. Tucson, Arizona: The University of Arizona Press. pp. 587–599.

Davis D. R., Weidenschilling S. J., Farinella P., Paplicchi P., and Binzel R. P. 1989. Asteroid collisional history: Effects on sizes and spins. In *Asteroids II*, edited by Binzel R. P., Gehrels T., and Matthews M. S. Tucson, Arizona: University of Arizona Press. pp. 805–826.

Fu R. R., Weiss B. P., Shuster D. L., Gattacceca J., Grove T. L., Suavet C., Lima E. A., Li L., and Kuan A. T. 2012. An ancient core dynamo in asteroid Vesta. *Science* 338:238–241.

Goodrich C. A., Kita N. T., Sutton S. R., Wirick S., and Gross J. 2017. The Miller Range 090340 and 090206 meteorites: Identification of new brachinite-like achondrites with implications for the diversity and petrogenesis of the brachinite clan. *Meteoritics & Planetary Science* 52:949–978.

Gopon P., Spicuzza M. J., Kelly T. F., Reinhard D., Prosa Ty J., and Fournelle J. 2017. Ultra-reduced phases in Apollo 16 regolith: Combined field emission electron probe microanalysis and atom probe tomography of submicron Fe-Si grains in Apollo 16 sample 61500. *Meteoritics & Planetary Science* 52:1941–1962.

Gu L., Zhang B., Hu S., Noguchi T., Hidaka H., and Lin Y. 2018. The discovery of silicon oxide nanoparticles in space-weathered of Apollo 15 lunar soil grains. *Icarus* 303:47–52.

Hapke B. 1973. Darkening of silicate rocks by solar wind sputtering. *Moon* 7:342–355.

Hapke B. 2001. Space weathering from Mercury to the main asteroid belt. *Journal of Geophysical Research: Planets* 106:10,039–10,073.

Hapke B., Cassidy W., and Wells E. 1975. Effects of vapor phase deposition processes on the optical, chemical and magnetic properties of the lunar regolith. *Moon* 13:339–353.

Harries D. and Langenhorst F. 2014. The mineralogy and space weathering of a regolith grain from 25143 Itokawa and the possibility of annealed solar wind damage. *Earth, Planets and Space* 66:163.

Harries D. and Langenhorst F. 2018. Carbide-metal assemblages in a sample returned from asteroid 25143 Itokawa: Evidence for methane-rich fluids during metamorphism. *Geochimica et Cosmochimica Acta* 222:53–73.

Harries D., Yakame S., Karouji Y., Uesugi M., and Langenhorst F. 2016. Secondary submicrometer impact cratering on the surface of asteroid 25143 Itokawa. *Earth and Planetary Science Letters* 450:337–345.

Hiroi T., Pieters C., and Takeda H. 1994. Grain size of the surface regolith of asteroid 4 Vesta estimated from its reflectance spectrum in comparison with HED meteorites. *Meteoritics* 29:394–396.

Joy K. H., Crawford I. A., Anand M., Greenwood R. C., Franchi I. A., and Russell S. S. 2008. The petrology and geochemistry of Miller Range 05035: A new lunar gabbro meteorite. *Geochimica et Cosmochimica Acta* 72:3822–3844.

Joy K. H., Zolensky M. E., Nagashima K., Huss G. R., Ross D. K., McKay D. S., and Kring D. A. 2012. Direct detection of projectile relics from the end of the lunar basin-forming epoch. *Science* 334:1426–1429.

Keller L. P. and Berger E. L. 2014. A transmission electron microscope study of Itokawa regolith grains. *Earth, Planets and Space* 66:71.

Keller L. P. and McKay D. S. 1997. The nature and origin of rims on lunar soil grains. *Geochimica et Cosmochimica Acta* 61:2331–2341.

Korotev R. L., Jolliff B. L., Zeigler R. A., Gillis J. J., and Haskin L. A. 2003. Feldspathic lunar meteorites and their implications for compositional remote sensing of the lunar surface and the composition of the lunar crust. *Geochimica et Cosmochimica Acta* 67:4895–4923.

Liu Y., Floss C., Day J. M. D., Hill E., and Taylor L. A. 2009. Petrogenesis of lunar mare basalt meteorite Miller Range 05035. *Meteoritics & Planetary Science* 44:261–284.

Liu Y., Keller L. P., Fraeman A. A., Christoffersen R., Rahman Z., Ehlmann B. L., Noble S. K., and Barrat J. A. 2015. Agglutinates in howardite 1769: Space weathering on Vesta (abstract #1706). 46th Lunar and Planetary Science Conference. CD-ROM.

McCord T. B., Adams J. B., and Johnson T. V. 1970. Asteroid Vesta: Spectral reflectivity and compositional implications. *Science* 168:1445–1447.

McCoy T. J., Beck A. W., Prettyman T. H., and Mittlefehldt D. W. 2015. Asteroid (4) Vesta: II. Exploring a geologically and geochemically complex world with the Dawn Mission. *Chemie der Erde—Geochemistry* 75:273–285.

McKay D. S., Heiken G., Basu A., Blanford G., Simon S., Reedy R., French B. M., and Papike J. 1991. The lunar regolith. In *Lunar sourcebook: A User's guide to the moon*, edited by Heiken G. H., Vaniman D. T., and French B. M.. Cambridge: Cambridge University Press. pp. 285–356.

McSween H. Y. Jr., Mittlefehldt D. W., Beck A. W., Mayne R. G., and McCoy T. J. 2011. HED meteorites and their relationship to the geology of Vesta and the Dawn Mission. *Space Science Review* 163:141–174.

Mittlefehldt D. W. 2015. Asteroid (4) Vesta: I. The howardite-eucrite-diogenite (HED) clan of meteorites. *Chemie der Erde—Geochemistry* 75:155–183.

Nakamura E., Makishima A., Moriguti T., Kobayashi K., Tanaka R., Kunihiro T., Tsujimori T., Sakaguchi C., Kitagawa H., Ota T., Yachi Y., Yada T., Abe M., Fujimura A., Ueno M., Mukai T., Yoshikawa M., and Kawaguchi J. 2012. Space environment of an asteroid preserved on micrograins returned by the Hayabusa spacecraft. *Proceedings of the National Academy of Sciences* 109:E624–E629.

Noble S. K., Keller L. P., and Pieters C. M. 2007. An experimental approach to understanding the optical effects of space weathering. *Icarus* 192:629–642.

Noble S. K., Keller L. P., and Pieters C. M. 2010. Evidence of space weathering in regolith breccias II: Asteroidal regolith breccias. *Meteoritics & Planetary Science* 45:2007–2015.

Noguchi T., Nakamura T., Kimura M., Zolensky M. E., Tanaka M., Hashimoto T., Konno M., Nakato A., Ogami T., Fujimura A., Abe M., Yada T., Mukai T., Ueno M., Okada T., Shirai K., Ishibashi Y., and Okazaki R. 2011. Incipient space weathering observed on the surface of Itokawa dust particles. *Science* 333:1121–1124.

Noguchi T., Kimura M., Hashimoto T., Konno M., Nakamura T., Zolensky M. E., Okazaki R., Tanaka M., Tsuchiyama A., Nakato A., Ogami T., Ishida H., Sagae R., Tsujimoto S., Matsumoto T., Matsuno J., Fujimura A., Abe M., Yada T., Mukai T., Ueno M., Okada T., Shirai K., and Ishibashi Y. 2014. Space weathered rims found on the surfaces of the Itokawa dust particles. *Meteoritics & Planetary Science* 49:188–214.

Pang R. L., Zhang A. C., and Wang R. C. 2017. Complex origins of silicate veinlets in HED meteorites: A case study of Northwest Africa 1109. *Meteoritics & Planetary Science* 52:2113–2131.

Papike J. J., Ryder G., and Shearer C. K. 1998. Lunar samples. In *Planetary materials*, edited by Papike J. J. Reviews in Mineralogy, vol. 36. Washington, D.C.: Mineralogical Society of America. pp. 5.1–5.234.

Papike J. J., Karner J. M., and Shearer C. K. 2003. Determination of planetary basalt parentage: A simple technique using the electron microprobe. *American Mineralogist* 88:469–472.

Patzer A. and McSween H. Y. 2012. Ordinary (mesostasis) and not-so-ordinary (symplectites) late-stage assemblages in howardites. *Meteoritics & Planetary Science* 47:1475–1490.

Pieters C. M. and Noble S. K. 2016. Space weathering on airless bodies. *Journal of Geophysical Research: Planets* 121:1865.

Pieters C. M., Taylor L., Noble S., Keller L., Hapke B., Morris R., Allen C. C., McKay D. S., and Wentworth S. 2000. Space weathering on airless bodies: Resolving a mystery with lunar samples. *Meteoritics & Planetary Science* 35:1101–1107.

Pieters C. M., Ammannito E., Blewett D. T., Denevi B. W., De Sanctis M. C., Gaffey M. J., Le Corre L., Li J. Y., Marchi S., McCord T. B., McFadden L. A., Mittlefehldt D. W., Nathues A., Palmer E., Reddy V., Raymond C. A., and Russell C. T. 2012. Distinctive space weathering on Vesta from regolith mixing processes. *Nature* 491:79–82.

Rubin A. E. 2015. Maskelynite in asteroidal, lunar and planetary basaltic meteorites: An indicator of shock pressure during impact ejection from their parent bodies. *Icarus* 257:221–229.

Russell C. T., Raymond C. A., Coradini A., McSween H. Y., Zuber M. T., Nathues A., De Sanctis M. C., Jaumann R., Konopliv A. S., Preusker F., Asmar S. W., Park R. S., Gaskell R., Keller H. U., Mottola S., Roatsch T., Scully J. E. C., Smith D. E., Tricarico P., Toplis M. J., Christensen U. R., Feldman W. C., Lawrence D. J., McCoy T. J., Prettyman T. H., Reedy R. C., Sykes M. E., and Titus T. N. 2012. Dawn at Vesta: Testing the protoplanetary paradigm. *Science* 33:684–686.

Shearer C. K., Burger P. V., Guan Y., Papike J. J., Sutton S. R., and Atudorei N. V. 2012. Origin of sulfide replacement

textures in lunar breccias. Implications for vapor element transport in the lunar crust. *Geochimica et Cosmochimica Acta* 83:138–158.

Taylor L. A., Patchen A., Mayne R. G., and Taylor D. H. 2004. The most reduced rock from the moon, Apollo 14 basalt 14053: Its unique features and their origin. *American Mineralogist* 89:1617–1624.

Thompson M. S., Christoffersen R., Zega T. J., and Keller L. P. 2014. Microchemical and structural evidence for space weathering in soils from asteroid Itokawa. *Earth, Planets and Space* 66:89.

Thompson M. S., Zega T. J., Becerra P., Keane J. T., and Byrne S. 2016. The oxidation state of nanophase Fe particles in lunar soil: Implications for space weathering. *Meteoritics & Planetary Science* 51:1082–1095.

Tomeoka K., Nomura K., and Takeda H. 1992. Na-bearing Ca-Al-rich inclusions in the Yamato-791717 CO carbonaceous chondrite. *Meteoritics* 27:136–143.

Wu Y., Li X., Yao W., and Wang S. 2017. Impact characteristics of different rocks in a pulsed laser irradiation experiment: Simulation of micrometeorite bombardment on the Moon. *Journal of Geophysical Research: Planets* 122:1956–1967.

Zhang A. C. and Yurimoto H. 2013. Petrography and mineralogy of the ungrouped type 3 carbonaceous chondrite Dar al Gani 978. *Meteoritics & Planetary Science* 48:1651–1677.

Zhang A. C., Wang R. C., Hsu W. B., and Bartoschewitz R. 2013. Record of S-rich vapors on asteroid 4 Vesta: Sulfurization in the Northwest Africa 2339 eucrite. *Geochimica et Cosmochimica Acta* 109:1–13.

Zhang A. C., Bu Y. F., Pang R. L., Sakamoto N., Yurimoto H., Chen L. H., Gao J. F., Du D. H., Wang X. L., and Wang R. C. 2018. Origin and implications of troilite-orthopyroxene intergrowths in the brecciated diogenite Northwest Africa 7183. *Geochimica et Cosmochimica Acta* 220:125–145.

Zolensky M. E., Weisberg M. K., Buchanan P. C., and Mittlefehldt D. W. 1996. Mineralogy of carbonaceous chondrite clasts in HED achondrites and the Moon. *Meteoritics & Planetary Science* 31:518–537.